Geochemical Perspectives Letters

The isotopic signature of U^V during bacterial reduction

A.R. Brown[1], M. Molinas[1], Y. Roebbert[2], R. Faizova[3], T. Vitova[4], A. Sato[5,6], M. Hada[5], M. Abe[5,6], M. Mazzanti[3], S. Weyer[2], R. Bernier-Latmani[1*]

OPEN ACCESS

https://doi.org/10.7185/geochemlet.2411

Abstract

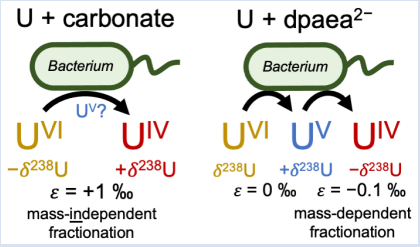

The two step electron transfer during bacterial reduction of U^{VI} to U^{IV} is typically accompanied by mass-independent fractionation of the ^{238}U and ^{235}U isotopes, whereby the heavy isotope accumulates in the reduced product. However, the role of the U^V intermediate in the fractionation mechanism is unresolved due to the challenges associated with its chemical stability. Here, we employed the U^V stabilising ligand, dpaea^{2-}, to trap aqueous U^V during U^{VI} reduction by *Shewanella oneidensis*. Whilst the first reduction step from U^{VI} to U^V displayed negligible fractionation, reduction of U^V to U^{IV} revealed mass-dependent isotope fractionation (preferential reduction of the ^{235}U), contrary to most previous observations. This surprising behaviour highlights the control that the U-coordinating ligand exerts over the balance between reactant U supply, electron transfer rate, and U^{IV} product sequestration, suggesting that U^V speciation should be considered when using U isotope ratios to reconstruct environmental redox conditions.

Received 13 July 2023 | Accepted 1 March 2024 | Published 9 April 2024

Introduction

Hexavalent uranium (U^{VI}) is the predominant oxidation state of U under ambient oxic conditions at Earth's surface and forms soluble uranyl complexes. Under anoxic conditions, reduction of U^{VI} to tetravalent U (U^{IV}) can be mediated by an array of microorganisms or abiotically *via* Fe(II)- or sulfide-bearing compounds (Basu *et al.*, 2014; Brown *et al.*, 2018), resulting in the precipitation of sparingly soluble U^{IV} species. This behaviour has been harnessed for the (bio)remediation of U contaminated groundwater.

Such U redox transformations are often accompanied by changes in the $^{238}U/^{235}U$ ratio, reported as $\delta^{238}U$ (Andersen *et al.*, 2017). Both *ab initio* calculations and isotope exchange experiments indicate that, at equilibrium, heavy ^{238}U is enriched in the U^{IV} oxidation state (Schauble, 2007; Abe *et al.*, 2008; Wang *et al.*, 2015). This mass-independent fractionation arises from the nuclear field shift effect (NFSE), due to differences in the size and shape of the nuclei of heavy element isotopologues (Bigeleisen, 1996; Schauble, 2007). At equilibrium, the NFSE is larger than, and operates in the opposite direction to, the conventional mass-dependent isotope effect, whereby the vibrational zero point energy of the lighter isotope leads to its enrichment in U^{IV} as mass-dependent fractionation (MDF) (Bigeleisen, 1996; Schauble, 2007; Fujii *et al.*, 2009). Thus, enrichment of ^{238}U in U^{IV} following U^{VI} reduction has also been attributed to a dominant NFSE (Weyer *et al.*, 2008; Basu *et al.*, 2014, 2020; Stirling *et al.*, 2015; Stylo *et al.*, 2015), despite not necessarily representing isotopic equilibrium conditions.

As U isotope fractionation is predominantly associated with redox transformations, U isotope signatures have been utilised as a (1) monitoring tool tuned specifically to the reductive rather than adsorptive removal of U^{VI} during remediation (Bopp *et al.*, 2010), and (2) palaeo-redox proxy, whereby the preferential reduction of ^{238}U during marine anoxia is recorded in sedimentary rocks and can be used to reconstruct the pervasiveness of anoxia in past global oceans (Montoya-Pino *et al.*, 2010; Brennecka *et al.*, 2011; Andersen *et al.*, 2017). Hence, it is crucial to constrain the mechanistic underpinnings of U isotope fractionation to improve the reliability of U isotope based redox reconstructions.

One important aspect of the U reduction mechanism is the role of the pentavalent U (U^V) intermediate. Previous studies have focused on the complete reduction of U^{VI} to U^{IV}. However, there is increasing evidence of the stabilisation and persistence of U^V intermediates within abiotic and biological systems (Roberts *et al.*, 2017; Pan *et al.*, 2020).

During microbiological U^{VI} reduction, two distinct mechanisms for the complete reduction to U^{IV} can occur: either *via* disproportionation of two uranyl^V atoms (generating U^{VI} and U^{IV}) (Vettese *et al.*, 2020), or *via* a second biologically mediated electron transfer to U^V (Molinas *et al.*, 2021, 2023). However, due to the challenges associated with the chemical stabilisation and

1. École Polytechnique Fédérale de Lausanne (EPFL), Environmental Microbiology Laboratory, CH-1015 Lausanne, Switzerland
2. Institute of Mineralogy, Leibniz University Hannover, D-30167 Hannover, Germany
3. École Polytechnique Fédérale de Lausanne (EPFL), Group of Coordination Chemistry, CH-1015 Lausanne, Switzerland
4. Karlsruhe Institute of Technology (KIT), Institute for Nuclear Waste Disposal (INE), D-76021 Karlsruhe, Germany
5. Department of Chemistry, Tokyo Metropolitan University, Tokyo, Japan
6. Department of Chemistry, Hiroshima University, Hiroshima, Japan
* Corresponding author (email: rizlan.bernier-latmani@epfl.ch)

separation of U^{V}, there is a lack of experimental evidence for its isotopic fractionation, and thus its role in the fractionation mechanism remains unresolved.

Ab initio calculations of the equilibrium isotope fractionation factor combined with a multi-step model of biological U^{VI}-carbonate reduction suggests that fractionation factors of up to 1.6 ‰ for the U^{VI} to U^{V} step and ~0.8 ‰ for the U^{V} to U^{IV} step (a total of ~2.4 ‰) may be expected (Sato *et al.*, 2021). However, these values are significantly larger than those observed in nature or experimentally for U^{VI} to U^{IV} reduction, and it is not clear whether and how redox transformations to and from the U^{V} intermediate are involved in this discrepancy.

The aminocarboxylate ligand $dpaea^{2-}$ ($dpaeaH_2$ = bis(pyridyl-6-methyl-2-carboxylate)-ethylamine) can be used to precipitate both U^{VI} and U^{IV} whilst maintaining U^{V} as an aqueous complex at circumneutral pH (Faizova *et al.*, 2018). These properties have allowed the reduction of U^{VI} by *Shewanella oneidensis* to be followed, revealing the potential for the biological reduction of the U^{V} intermediate, rather than its disproportionation (Molinas *et al.*, 2021, 2023).

Here, we leveraged the characteristics of $dpaea^{2-}$ to trap aqueous U^{V} and provide direct experimental evidence of the U^{V} isotope signature during biological reduction by *S. oneidensis*. The observed isotopic fractionation factors were then compared to those predicted for equilibrium both computationally, using *ab initio* calculations, and experimentally, using isotope exchange approaches (see Supplementary Information for details).

Results and Discussion

The overall experimental flow entails the biological reduction of U^{VI}-dpaea to first U^{V}-dpaea and then of U^{V}-dpaea to U^{IV}-dpaea. The temporal separation of the two steps, made possible by the vastly different reduction rates, allows the investigation of the isotopic fractionation of one step and then the other. Additionally, the equilibrium isotope fractionation factor was calculated *via ab initio* calculations. Finally, to investigate the equilibrium isotopic fractionation of U^{V}-dpaea and U^{IV}-dpaea, a heavy U^{V}-dpaea was incubated with a light U^{IV}-dpaea and the isotopic exchange probed over time.

First, U^{VI}-dpaea was produced and reduced biologically. We incubated *S. oneidensis* with solid phase $U^{VI}O_2$-dpaea and observed a rapid decrease in U^{VI} over 24 hr. This was concomitant with an increase in aqueous U (Fig. 1a) comprising predominantly U^{V} (Fig. 1b) that was not observed in abiotic controls (Fig. S-1). Acidification of the aqueous U in 4.5 N HCl, in preparation for ion exchange chromatography, led to the detection of approximately equal quantities of U^{VI} and U^{IV} after separation (Fig. S-2), indicative of U^{V} disproportionation in the acidified preparation. Collectively, these data suggest that the first electron transfer was achieved rapidly, leading to the accumulation of U^{V} in solution, in agreement with previous studies (Molinas *et al.*, 2021, 2023).

Aqueous U^{V} reached its maximum after 24 hr, after which the concentration decreased steadily over fifty days, concomitant with an increase in solid phase U^{IV} (Fig 1a). This suggests that the second electron transfer proceeds much more slowly than the first. Previous work confirms that reduction from U^{V} to U^{IV} is indeed mediated by electron transfer from *S. oneidensis*, as opposed to U^{V} disproportionation (Molinas *et al.*, 2021, 2023). It is likely that reduction of $U^{VI}O_2$-dpaea proceeds *via* dissolution of the solid uranyl^{VI} followed by rapid reduction of aqueous uranyl^{VI}, *i.e.* dissolution is the rate limiting step for the first electron transfer (Molinas *et al.*, 2023).

A slow second electron transfer step (U^{V}/U^{IV}) is consistent with abiotic reduction by sodium hydrosulfite (Faizova *et al.*, 2020). Cyclic voltammograms of a $U^{V}O_2$-dpaea complex at pH 7 did not display a U^{V}/U^{IV} reduction event, suggesting slow electron transfer kinetics that may be related to required structural re-arrangements for the formation of a tri-nuclear U^{IV} product (Faizova *et al.*, 2018, 2020).

Uranium isotopic fractionation during the first electron transfer from U^{VI} to U^{V} was investigated with a dedicated incubation of $U^{VI}O_2$-dpaea (Fig. 2a). Here, the increasing aqueous U showed negligible changes in $\delta^{238}U$, indicating that the U^{VI}/U^{V} reduction displayed little fractionation (Fig. 2b). Reduction of U^{VI} by a range of bacterial species typically display enrichment of the heavier ^{238}U in the reduced product, consistent with the predictions of NFS theory during equilibrium isotope fractionation (Basu *et al.*, 2014). Indeed, *ab initio* calculation of the expected isotope fractionation factor between the $U^{VI}O_2$-dpaea and $U^{V}O_2$-$dpaea^{-}$ at equilibrium gave a value of 0.82–1.60 ‰ (Table S-1), wherein the positive value signals preferential reduction of ^{238}U. Rather, the isotope signatures of the $U^{V}O_2$-$dpaea^{-}$ observed in the experiment appear consistent with dissolution being the rate limiting step for the first electron transfer, such that U isotope reduction is rapid and quantitative. As dissolution does not involve a redox reaction, the mass-independent isotope fractionation predicted by the NFSE would not be expected.

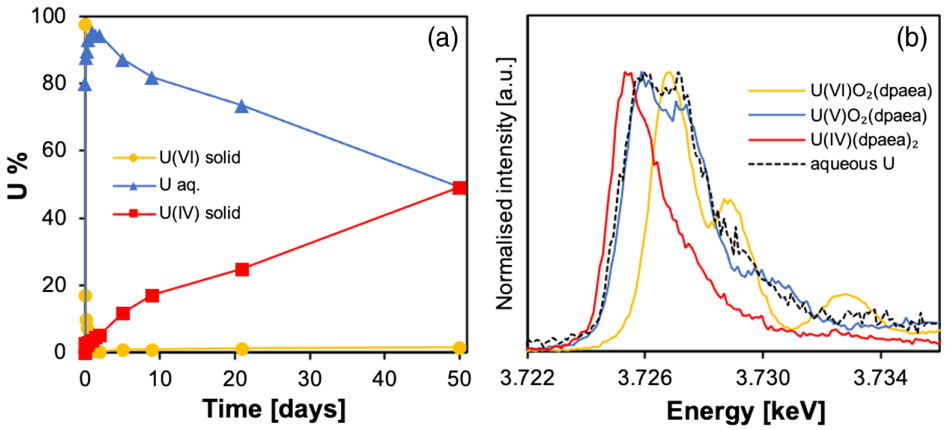

Figure 1 **(a)** Uranium mass distribution in sacrificial reactors containing *S. oneidensis* incubated with $U^{VI}O_2$-dpaea. **(b)** Normalised U M_4-edge HR-XANES spectrum of aqueous uranium after 144 hr of incubation with *S. oneidensis*, along with $U^{VI}O_2$-dpaea, $U^{V}O_2$-$dpaea^{-}$ and U^{IV}-$(dpaea)_2$ standards.

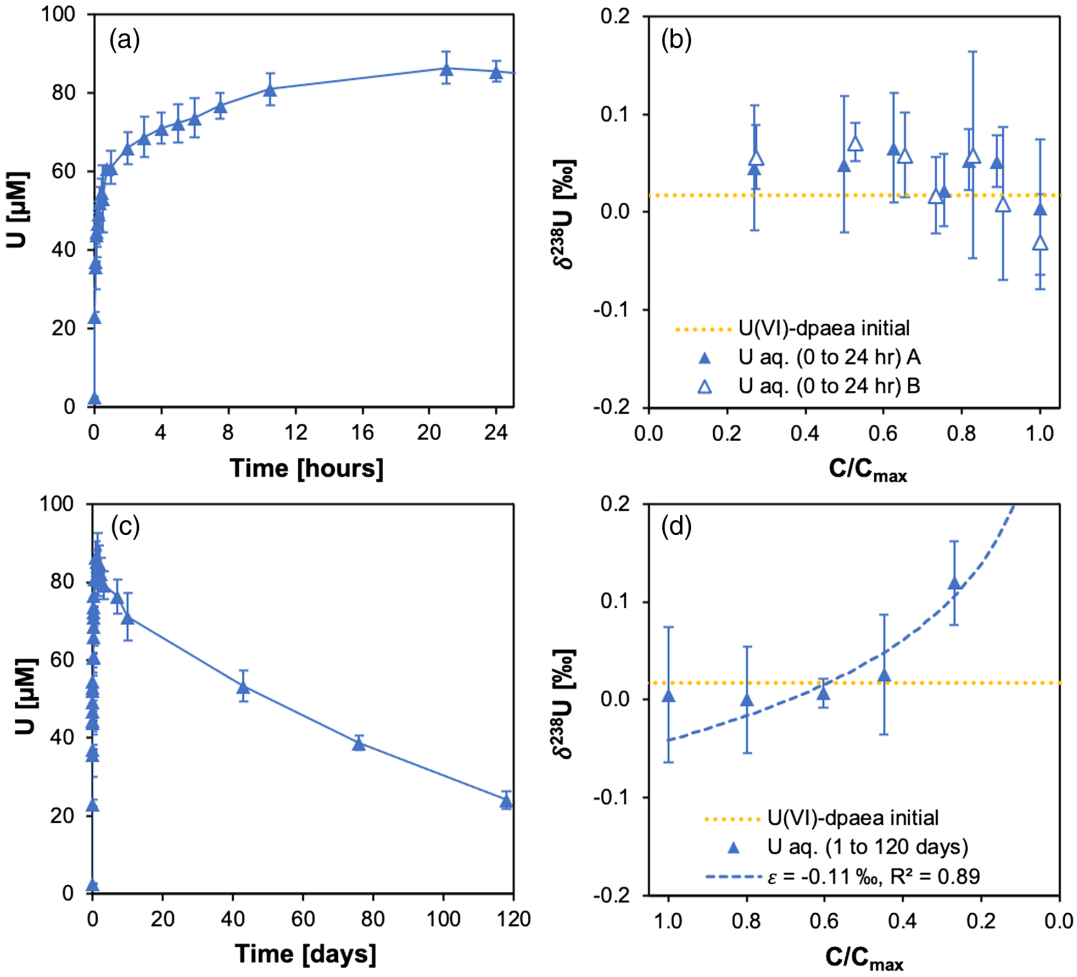

Figure 2 **(a)** Aqueous uranium concentrations throughout the first 24 hr of incubation of $U^{VI}O_2$-dpaea and *S. oneidensis*. Symbols and error bars depict one standard deviation of the mean of duplicate reactors. **(b)** Corresponding $\delta^{238}U$ values of the aqueous U in duplicate systems (A and B), reported as a fraction of the maximum aqueous U concentration. Symbols and error bars depict two standard deviations of the mean of triplicate measurements. The $\delta^{238}U$ value of the initial $U^{VI}O_2$-dpaea is plotted as a yellow dotted line. **(c)** Aqueous uranium concentrations throughout the whole reaction between $U^{VI}O_2$-dpaea and *S. oneidensis*. Symbols and error bars depict one standard deviation of the mean of duplicate reactors. **(d)** $\delta^{238}U$ values of the aqueous U after 24 hr when the aqueous U concentration began to decrease. Values are reported as a fraction of the maximum aqueous U concentration. Symbols and error bars depict two standard deviations of the mean of triplicate measurements. The Rayleigh model (blue dashed line) corresponds to the linear best fit of the logarithmic data, $R^2 = 0.89$, from which the isotope enrichment factor, ε, is derived.

Once U^{VI} was completely reduced and aqueous U^{V} reached its maximum concentration after 24 hr, the isotope signature of the aqueous U^{V} was measured to quantify fractionation during the U^{V}/U^{IV} reduction step (Figs. 2d, S-3). Although limited fractionation was observed, Rayleigh distillation models could be fitted to the data, indicating fractionation factors (ε) of −0.10 ‰ and −0.11 ‰ for the two batch replicates. These negative values indicate the preferential accumulation of lighter ^{235}U in the reduced product, contrary to previous observations for microbial U^{VI} reduction and at odds with NFS theory (Basu *et al.*, 2014; Stirling *et al.*, 2015; Stylo *et al.*, 2015). To ascertain whether this direction of fractionation reflected equilibrium in the peculiar case of a strong aminocarboxylate ligand, we performed *ab initio* calculations of the fractionation factor at equilibrium between $U^{V}O_2$-dpaea^{-} and either U^{IV}-$(dpaea)_2$ or a non-uraninite U^{IV} species, the two likely products of this biological reaction (Molinas *et al.*, 2021). We modelled the non-uraninite U^{IV} as a cluster of ningyoite ($CaU(PO_4)_2$), a close analogue of the non-crystalline biotic reduction products (Bernier-Latmani *et al.*, 2010; Alessi *et al.*, 2014). The fractionation factors of 0.27–0.33 ‰ for the U^{IV}-$(dpaea)_2$ product and 0.13–0.46 ‰ for ningyoite both reveal that ^{238}U would be enriched in the U^{IV} product at equilibrium (Table S-1), contrary to that observed during biological reduction. These calculations indicate that the bioreduction system was far from equilibrium and suggest that the reaction mechanism precluded the full expression of NFSE that would have enriched ^{238}U in the product. Furthermore, recent work has proposed that slow microbial reduction should impart significant mass-independent fractionation of up to +1 ‰ (Brown *et al.*, 2018; Basu *et al.*, 2020), whereas negative fractionation factors are typically only observed for rapid abiotic reductions, on the order of hours (Stylo *et al.*, 2015). The slow reduction of the $U^{V}O_2$-dpaea^{-} observed in our experiments (on the order of months), suggests that the proposed reduction rate-fractionation relationship does not hold for all circumstances.

To investigate whether equilibrium isotope exchange and the associated expression of the NFSE could overprint the reduction-derived MDF signature, we performed isotope exchange experiments between the solid U^{IV} product of the bioreduction experiment, with an initial (light) $\delta^{238}U$ of 0 ‰, and aqueous $U^{V}O_2$-dpaea^{-}, with an initial (heavy) $\delta^{238}U$ of ~5 ‰. Over 200

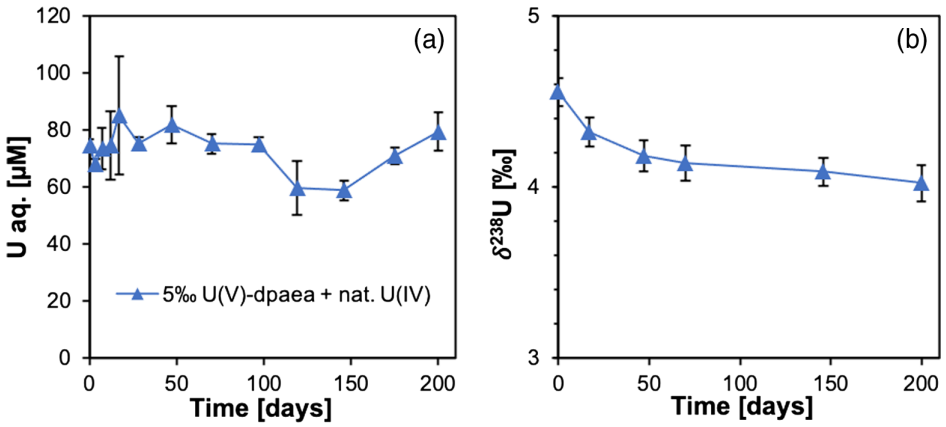

Figure 3 **(a)** Aqueous uranium concentrations during equilibrium isotope exchange experiments between $U^{V}O_2$-dpaea$^-$ with an initial isotopic composition of ~5 ‰, and U^{IV} present as the product of the bioreduction experiments of natural U, with an initial isotopic composition of 0 ‰. Symbols and error bars depict one standard deviation of the mean of duplicate reactors. **(b)** $\delta^{238}U$ values of the aqueous U. Symbols and error bars depict one standard deviation of the mean of duplicate reactors.

days, aqueous U became isotopically lighter by 0.6 ‰, indicating the preferential accumulation of ^{238}U in the U^{IV} solid (Fig. 3). Whilst this direction of fractionation is in agreement with that calculated for equilibrium, isotope mass balance calculations indicate that the U^{IV} solid did not become heavier than the aqueous U^{V}, contrary to the computed equilibrium. These data show that progress to full equilibrium is significantly limited over the course of the experiment, presumably due to slow ligand exchange kinetics.

This hypothesis is consistent with the strong pentadentate coordination of U^{V} by dpaea, which provides protection from ligand dissociation and cation-cation interactions typical of U^{V} disproportionation (Faizova *et al.*, 2018). Furthermore, any preferential re-oxidation of $^{235}U^{IV}$ to U^{V} would require the *de novo* formation of the two uranyl dioxo bonds and re-coordination with dpaea. This is likely kinetically limited due to steric hinderance by the U^{IV} coordinating ligands. Therefore, we propose that isotope signatures indicating mass-dependent fractionation (faster reaction of ^{235}U) are preserved during the biological reduction of $U^{V}O_2$-dpaea$^-$ because subsequent equilibrium isotope exchange, fractionating in the opposite direction, is limited.

Regardless of the abiotic equilibrium isotope exchange between reactants and products (independent of the bioreduction reaction), a recent model has demonstrated the importance of back reaction within the U^{VI} bioreduction pathway in controlling the overall isotope fractionation (Sato *et al.*, 2021). The model stipulates that the overall isotope fractionation at each reaction step arises from the balance between the forward and backward reaction rates, and the attendant isotope fractionation for the forward and backward reactions. As such, reactions with equal forward and backward reaction rates will display the full fractionation factor predicted for equilibrium (typically positive for U reduction, indicating preferential accumulation of ^{238}U in the product). On the other hand, irreversible reactions will result in no observed fractionation. The theory of this model has been demonstrated experimentally during U^{VI} reduction by *S. oneidensis*, in which back reaction (reverse electron transfer) was limited by large electron fluxes from oxidation of the electron donor (Brown *et al.*, 2023a). These systems result in significantly less isotope fractionation than those with small electron fluxes, which permit more back reaction. The theoretical model and associated experimental evidence, coupled to our observations of the isotope exchange experiment, would suggest that back reaction during biological reduction of $U^{V}O_2$-dpaea$^-$ is limited and point toward the role of the U coordinating ligand in controlling the magnitude of isotope fractionation.

Furthermore, during microbiological reduction of U^{VI}-carbonate, the conventional isotopic mass effect was fully expressed, while the NFSE was not (Brown *et al.*, 2023b). This implies that the mass-dependent vibrational effect and the mass-independent NFSE are two competing effects operating in opposing directions and is consistent with the proposal that the NFSE requires reaction reversibility in order to overprint the mass-dependent effect.

Collectively, these studies indicate that the inhibition of back reaction in the dpaea system is so severe that the mass-dependent isotope fractionation factor is preserved. More specifically, we propose the following mechanism: first, the flux of electrons from the cell to the outer membrane U-reducing proteins is significantly greater than the U^{V} reduction rates (limited by either low redox potential and/or steric hinderance) (Fig. 4). This allows the redox-active Fe-bearing heme groups of these proteins to become fully reduced prior to electron transfer to U^{V}. Eventually, electron transfer from the heme Fe^{II} to U^{V} occurs with isotopic fractionation according to the conventional mass effect – faster reaction of ^{235}U. Concurrently, a rapid continuous flux of electrons from metabolism re-reduces the Fe^{III} of the

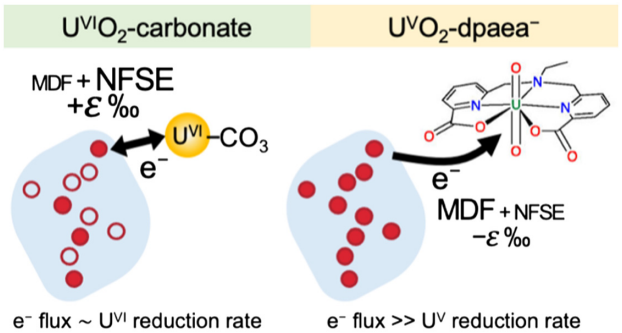

Figure 4 Cartoon of the proposed mechanism of U isotope reduction and fractionation for both U^{VI}-carbonate (left) and U^{V}-dpaea$^-$ (right). Electrons are transferred from the cell to outer membrane U reducing proteins (blue areas) containing multiple redox active heme iron centres (red circles). Depending on the flux of electrons, the heme iron centres are either in their reduced state (solid fill) or oxidised state (open fill).

heme group (empty circles in Fig. 4) and prevents reverse electron transfer from the newly reduced U^{IV}. Consequently, isotopic equilibration that is dominated by the mass-independent NFSE cannot over-print the initial MDF, unlike in U-carbonate containing systems.

Likewise, back reaction may also be limited by U^{IV} sequestration, *i.e.* kinetic limitations imposed by the U^{IV} structure and bond rearrangement to recover the uranyl bond structure, resulting in significantly faster electron transfer rates from the heme Fe^{II} to $U^{V}O_2$-dpaea$^-$ than U^{IV} to heme Fe^{III}.

Conclusions

We employed the U^{V} stabilising ligand, dpaea, to trap aqueous U^{V} and observed, for the first time, the isotopic signature of U^{V} throughout the bioreduction of U^{VI} to U^{IV}. Whilst the observation of a mass-dependent isotope fractionation factor appears to conflict with previous studies of microbial U reduction, this is likely not an artefact of the unique properties of dpaea (*i.e.* its ability to solubilise and trap U^{V}). Rather, these adventitious properties have elucidated the control U coordinating ligands exert over the balance between reactant U supply, electron transfer rate, and U^{IV} product sequestration. Thus, we infer that other ligands (that cannot stabilise U^{V}) will behave similarly when such conditions are met. This has significant implications for the interpretation of U isotope signatures in environments where the availability of high affinity ligands may impact U lability. For example, in reducing environments with considerable amounts of organic carbon (providing both a source of electrons for microbial U^{VI} reduction and a supply of organic complexants), the contribution of the NFSE to observed isotopic signatures may be diminished. This may lead to false interpretations of U isotope signatures, *e.g.*, in applications using organic-rich anoxic sediments as a palaeo-redox archive. In such studies, the observation of lower $\delta^{238}U$ (arising from NFSE-dominated mass-independent fractionation) is usually thought to indicate either a local shift in depositional conditions or water column stratification (Andersen *et al.*, 2017; Brüske *et al.*, 2020; Lau *et al.*, 2022), or a shift in the U isotope mass balance, resulting from enhanced oceanic anoxic environments at regional or global scales (Montoya-Pino *et al.*, 2010; Andersen *et al.*, 2017). However, our results show that the extent and direction of U isotope fractionation during U reduction may depend on the stabilisation of U^{V} and, more generally, the lability of U complexes.

Furthermore, this study suggests that full expression of isotopic equilibrium in nature may be precluded by U speciation, in addition to the previous roles reported for electron flux and U supply dynamics (Basu *et al.*, 2020; Brown *et al.*, 2023a). Future work should focus on delineating these controls with an aim to incorporate U speciation as a parameter within models of U isotope fractionation in the environment.

Acknowledgements

Funding for this work was provided by an ERC consolidator grant awarded to RB-L (725675: UNEARTH: "Uranium isotope fractionation: a novel biosignature to identify microbial metabolism on early Earth"). This work was also supported by JSPS KAKENHI Grant Numbers JP19K22171, JP21H01864 and JP22J12551. A part of the calculations was performed at the Research Center for Computational Science, Okazaki, Japan (Project: 21-IMS-C049 and 22-IMS-C049). Pierre Rossi provided invaluable support in complying with radiological safety regulations in the lab. We also thank two reviewers and the editor, Claudine Stirling, for their constructive input.

Editor: Claudine Stirling

Additional Information

Supplementary Information accompanies this letter at https://www.geochemicalperspectivesletters.org/article2411.

Cite this letter as: Brown, A.R., Molinas, M., Roebbert, Y., Faizova, R., Vitova, T., Sato, A., Hada, M., Abe, M., Mazzanti, M., Weyer, S., Bernier-Latmani, R. (2024) The isotopic signature of U^{V} during bacterial reduction. *Geochem. Persp. Let.* 29, 45–50. https://doi.org/10.7185/geochemlet.2411

References

Abe, M., Suzuki, T., Fujii, Y., Hada, M., Hirao, K. (2008) An *ab initio* molecular orbital study of the nuclear volume effects in uranium isotope fractionations. *The Journal of Chemical Physics* 129, 164309. https://doi.org/10.1063/1.2992616

Alessi, D.S., Lezama-Pacheco, J.S., Stubbs, J.E., Janousch, M., Bargar, J.R., Persson, P., Bernier-Latmani, R. (2014) The product of microbial uranium reduction includes multiple species with U(IV)-phosphate coordination. *Geochimica et Cosmochimica Acta* 131, 115–127. https://doi.org/10.1016/j.gca.2014.01.005

Andersen, M.B., Stirling, C.H., Weyer, S. (2017) Uranium Isotope Fractionation. *Reviews in Mineralogy and Geochemistry* 82, 799–850. https://doi.org/10.2138/rmg.2017.82.19

Basu, A., Sanford, R.A., Johnson, T.M., Lundstrom, C.C., Löffler, F.E. (2014) Uranium isotopic fractionation factors during U(VI) reduction by bacterial isolates. *Geochimica et Cosmochimica Acta* 136, 100–113. https://doi.org/10.1016/j.gca.2014.02.041

Basu, A., Wanner, C., Johnson, T.M., Lundstrom, C., Sanford, R.A., Sonnenthal, E., Boyanov, M.I., Kemner, K.M. (2020) Microbial U isotope fractionation depends on U(VI) reduction rate. *Environmental Science and Technology* 54, 2295–2303. https://doi.org/10.1021/acs.est.9b05935

Bernier-Latmani, R., Veeramani, H., Vecchia, E.D., Junier, P., Lezama-Pacheco, J.S., Suvorova, E.I., Sharp, J.O., Wigginton, N.S., Bargar, J.R. (2010) Non-uraninite products of microbial U (VI) reduction. *Environmental Science and Technology* 44, 9456–9462. https://doi.org/10.1021/es101675a

Bigeleisen, J. (1996) Nuclear size and shape effects in chemical reactions. Isotope chemistry of the heavy elements. *Journal of the American Chemical Society* 118, 3676–3680. https://doi.org/10.1021/ja954076k

Bopp, C.J., Lundstrom, C.C., Johnson, T.M., Sandford, R.A., Long, P.E., Williams, K.H. (2010) Uranium $^{238}U/^{235}U$ isotope ratios as indicators of reduction: Results from an *in situ* biostimulation experiment at Rifle, Colorado, U.S.A. *Environmental Science and Technology* 44, 5927–5933. https://doi.org/10.1021/es100643v

Brennecka, G.A., Herrmann, A.D., Algeo, T.J., Anbar, A.D. (2011) Rapid expansion of oceanic anoxia immediately before the end-Permian mass extinction. *Proceedings of the National Academy of Sciences of the United States of America* 108, 17631–17634. https://doi.org/10.1073/pnas.1106039108

Brown, S.T., Basu, A., Ding, X., Christensen, J.N., DePaolo, D.J. (2018) Uranium isotope fractionation by abiotic reductive precipitation. *Proceedings of the National Academy of Sciences of the United States of America* 115, 8688–8693. https://doi.org/10.1073/pnas.1805234115

Brown, A.R., Molinas, M., Roebbert, Y., Sato, A., Abe, M., Weyer, S., Bernier-Latmani, R. (2023a) Electron flux is a key determinant of uranium isotope fractionation during bacterial reduction. *Communications Earth and Environment* 4, 329. https://doi.org/10.1038/s43247-023-00989-x

Brown, A.R., Roebbert, Y., Sato, A., Hada, M., Abe, M., Weyer, S., Bernier-Latmani, R. (2023b) Contribution of the nuclear field shift to kinetic

uranium isotope fractionation. *Geochemical Perspectives Letters* 27, 43–47. https://doi.org/10.7185/geochemlet.2333

Brüske, A., Weyer, S., Zhao, M.Y., Planavsky, N.J., Wegwerth, A., Neubert, N., Dellwig, O., Lau, K.V., Lyons, T.W. (2020) Correlated molybdenum and uranium isotope signatures in modern anoxic sediments: Implications for their use as paleo-redox proxy. *Geochimica et Cosmochimica Acta* 270, 449–474. https://doi.org/10.1016/j.gca.2019.11.031

Faizova, R., Scopelliti, R., Chauvin, A.-S., Mazzanti, M. (2018) Synthesis and characterization of a water stable uranyl(V) complex. *Journal of the American Chemical Society* 140, 13554–13557. https://doi.org/10.1021/jacs.8b07885

Faizova, R., Fadaei-Tirani, F., Bernier-Latmani, R., Mazzanti, M. (2020) Ligand-supported facile conversion of uranyl(VI) into uranium(IV) in organic and aqueous media. *Angewandte Chemie* 132, 6822–6825. https://doi.org/10.1002/ange.201916334

Fujii, T., Moynier, F., Albarède, F. (2009) The nuclear field shift effect in chemical exchange reactions. *Chemical Geology* 267, 139–156. https://doi.org/10.1016/j.chemgeo.2009.06.015

Lau, K.V, Hancock, L.G., Severmann, S., Kuzminov, A., Cole, D.B., Behl, R.J., Planavsky, N.J., Lyons, T.W. (2022) Variable local basin hydrography and productivity control the uranium isotope paleoredox proxy in anoxic black shales. *Geochimica et Cosmochimica Acta*. 317, 433–456. https://doi.org/10.1016/j.gca.2021.10.011

Molinas, M., Faizova, R., Brown, A., Galanzew, J., Schacherl, B., Bartova, B., Meibom, K.L., Vitova, T., Mazzanti, M. and Bernier-Latmani, R. (2021) Biological reduction of a U(V)-organic ligand complex. *Environmental Science and Technology* 55, 4753–4761. https://doi.org/10.1021/acs.est.0c06633

Molinas, M., Meibom, K.L., Faizova, R., Mazzanti, M., Bernier-Latmani, R. (2023) Mechanism of reduction of aqueous U(V)-dpaea and solid-phase U(VI)-dpaea complexes: The role of multiheme *c*-type cytochromes. *Environmental Science and Technology* 57, 7537–7546. https://doi.org/10.1021/acs.est.3c00666

Montoya-Pino, C., Anbar, A.D., van de Schootbrugge, B., Oschmann, W., Pross, J., Arz, H.W., Weyer, S. (2010) Global enhancement of ocean anoxia during Oceanic Anoxic Event 2: A quantitative approach using U isotopes. *Geology* 38, 315–318. https://doi.org/10.1130/G30652.1

Pan, Z., Bártová, B., Lagrange, T., Butorin, S.M., Hyatt, N.C., Stennett, M.C., Kvashnina, K.O., Bernier-latmani, R. (2020) Nanoscale mechanism of UO_2 formation through uranium reduction by magnetite. *Nature Communications* 11, 1–12. https://doi.org/10.1038/s41467-020-17795-0

Roberts, H.E., Morris, K., Law, G.T.W., Mosselmans, J.F.W., Bots, P., Kvashnina, K., Shaw, S. (2017) Uranium(V) incorporation mechanisms and stability in Fe(II)/Fe(III) (oxyhydr)oxides. *Environmental Science and Technology Letters* 4, 421–426. https://doi.org/10.1021/acs.estlett.7b00348

Sato, A., Bernier-Latmani, R., Hada, M., Abe, M. (2021) *Ab initio* and steady-state models for uranium isotope fractionation in multi-step biotic and abiotic reduction. *Geochimica et Cosmochimica Acta* 307, 212–227. https://doi.org/10.1016/j.gca.2021.05.044

Schauble, E.A. (2007) Role of nuclear volume in driving equilibrium stable isotope fractionation of mercury, thallium, and other very heavy elements. *Geochimica et Cosmochimica Acta* 71, 2170–2189. https://doi.org/10.1016/j.gca.2007.02.004

Stirling, C.H., Andersen, M.B., Warthmann, R., Halliday, A.N. (2015) Isotope fractionation of ^{238}U and ^{235}U during biologically-mediated uranium reduction. *Geochimica et Cosmochimica Acta* 163, 200–218. https://doi.org/10.1016/j.gca.2015.03.017

Stylo, M., Neubert, N., Wang, Y., Monga, N., Romaniello, S.J., Weyer, S., Bernier-Latmani, R. (2015) Uranium isotopes fingerprint biotic reduction. *Proceedings of the National Academy of Sciences of the United States of America* 112, 5619–24. https://doi.org/10.1073/pnas.1421841112

Vettese, G.F., Morris, K., Natrajan, L.S., Shaw, S., Vitova, T., Galanzew, J., Jones, D.L. and Lloyd, J.R. (2020) Multiple lines of evidence identify U(V) as a key intermediate during U(VI) reduction by *Shewanella oneidensis* MR1. *Environmental Science and Technology* 54, 2268–2276. https://doi.org/10.1021/acs.est.9b05285

Wang, X., Johnson, T.M., Lundstrom, C.C. (2015) Low temperature equilibrium isotope fractionation and isotope exchange kinetics between U(IV) and U(VI). *Geochimica et Cosmochimica Acta* 158, 262–275. https://doi.org/10.1016/j.gca.2015.03.006

Weyer, S., Anbar, A.D., Gerdes, A., Gordon, G.W., Algeo, T.J., Boyle, E.A. (2008) Natural fractionation of $^{238}U/^{235}U$. *Geochimica et Cosmochimica Acta* 72, 345–359. https://doi.org/10.1016/j.gca.2007.11.012

Geochemical Perspectives Letters

The isotopic signature of U^{V} during bacterial reduction

A.R. Brown, M. Molinas, Y. Roebbert, R. Faizova, T. Vitova, A. Sato, M. Hada, M. Abe, M. Mazzanti, S. Weyer, R. Bernier-Latmani

Supplementary Information

The Supplementary Information includes:

- Experimental Section
- Figures S-1 to S-3
- Table S-1
- Supplementary Information References

Experimental Section

Synthesis of natural U^{VI}-dpaea

Solid phase $U^{VI}O_2$-dpaea was synthesised as described previously (Faizova *et al.*, 2018). Briefly, natural U from an IRMM-184 nitrate stock was reacted with H_2dpaea in methanol and then evaporated to dryness. The powder was then transferred to an anoxic chamber (100% N_2, <0.1 ppm O_2; MBraun, Germany) and stored in the dark.

Cultivation of *Shewanella oneidensis*

To follow the reduction and fractionation of U^{VI}-dpaea, a high biomass inoculum of *Shewanella oneidensis* MR-1 was obtained by first growing it in oxic Luria-Bertani (LB) medium to mid-late exponential phase. The biomass was harvested by centrifugation for 10 min at 5000×*g* and was washed three times in an anoxic and sterile buffer that was modified from a Widdel low phosphate (WLP) medium to exclude carbonate and phosphate as potential U complexing agents. The composition was as follows: 0.68 mM $CaCl_2.2H_2O$, 6.71 mM KCl, 2.46 $MgCl_2.6H_2O$, 85.56 mM NaCl, 4.67 mM NH_4Cl 4.67 and 20 mM piperazine-N,N′-bis(2-ethanesulfonic acid) (PIPES) at pH 7.3.

Reduction of U^{VI}-dpaea by *S. oneidensis*

U^{VI}-dpaea reduction was followed under non-growth conditions with 20 mM sodium lactate serving as the electron donor. Here, aliquots of the washed cell suspension were added to anoxic and sterile reactors containing the modified WLP medium and ~130 µM U (equivalent aqueous concentration) as solid phase U^{VI}-dpaea powder. U reduction experiments were performed in two batches. The first was performed as a series of sacrificial reactors, allowing all the U oxidation states (solid U^{VI}, aqueous U^{V} and solid U^{IV}) to be successfully separated and quantified by anion exchange chromatography (see below). The aqueous U was separated from the solid phase by centrifugation at 12000×*g* for 10

min, followed by filtration of the supernatant through 0.22 µm PTFE filters. The solid phase was then acidified in 6 N HCl and immediately added to anion exchange columns for separation of U^{VI} and U^{IV} oxidation states. The second batch was performed in duplicate reactors and only the aqueous U was separated and quantified, in order to confirm the findings of the first sacrificial reactor batch experiment.

Anion exchange chromatography

In order to quantify U^{VI} reduction and isotope signatures over time in all experiments, U^{VI} was separated from total U using an anion exchange chromatography protocol adapted from Stoliker et al. (Stoliker *et al.*, 2013a, 2013b) and used previously (Molinas *et al.*, 2021, 2023). Briefly, strongly basic anion exchange resin (Dowex 1X8; 100−200 mesh) was added to polypropylene chromatographic columns to a bed volume of 2.5 mL. The resin was then preconditioned with 4.5 N HCl prior to addition of a U-containing sample that had been acidified to 4.5 N HCl. First, the U^{IV} fraction was eluted with 10 consecutive bed volumes of 4.5 N HCl, followed by elution of U^{VI} with 10 bed volumes of 0.1 N HCl. All steps were performed inside an anoxic chamber with Ultra-pure reagents that were flushed with nitrogen for more than 2 h before use. After separation, U concentrations in each fraction were quantified using ICP-MS. Previous studies observed isotopic cross-contamination between the two U oxidation states and thus applied a correction factor to the measured $\delta^{238}U$ (Wang *et al.*, 2015a, 2015b). However, our own tests, using the conditions above, showed negligible cross-contamination and no correction factor was required.

U isotope ratio analysis

Sample preparation for U isotope measurements were performed as described previously (Brown *et al.*, 2023), except that, prior to purification on Eichrom UTEVA resins, a weighed aliquot of the $^{236}U/^{233}U$ double spike solution (IRMM 3636-A, $^{236}U/^{233}U = 0.98130$) was added to the samples in order to correct for isotope fractionation during U purification and instrumental mass discrimination during MC-ICP-MS analysis (Richter *et al.*, 2008; Weyer *et al.*, 2008). Spike/sample mixtures for all samples and standards were adjusted to similar ratios ($^{236}U/^{235}U \approx 3 \pm 10\%$) to minimize peak tailing effects (from the ion beams of ^{238}U on ^{236}U and of ^{236}U on ^{235}U).

For sample analysis, two sample measurements were bracketed by two standard measurements and all samples and standards were measured with ~4 min total integration time. Mass bias correction was performed with the IRMM 3636 double spike (Richter *et al.*, 2008) and the exponential law (Russell *et al.*, 1978).

As before, isotope signatures are presented in the delta notation relative to the IRMM-184 U standard:

$$\delta^{238}U = \left[\frac{(^{238}U/^{235}U)_{sample}}{(^{238}U/^{235}U)_{standard}} - 1\right] \cdot 1000 \quad [‰] \qquad \text{(Eq. S-1)}$$

Rayleigh distillation models

Rayleigh distillation models were used to determined isotope fractionation factors (ε) using the method described previously (Brown *et al.*, 2023; Scott *et al.*, 2004).

***Ab initio* calculation of ε^{eq} between U^{VI} and U^{IV}**

We modelled the U^{VI} and U^{V} species as the dpaea complexes UO_2-dpaea and UO_2-dpaea$^-$, respectively, using the structures reported previously (Faizova *et al.*, 2018). The U^{IV} product was modelled as either U^{IV}-$(dpaea)_2$ or a non-uraninite U^{IV} species, the two likely products of this biological reaction (Molinas *et al.*, 2021). The non-uraninite U^{IV}

was modelled as a cluster of ningyoite ($H_{26}CaU(PO_4)_{10}^{2+}$), as established previously (Sato *et al.*, 2021), which is a close analogue of the non-crystalline biotic reduction products (Alessi *et al.*, 2014; Bernier-Latmani *et al.*, 2010; Sato *et al.*, 2021).

Calculations were performed as described previously (Brown *et al.*, 2023). The nuclear mass term, $\ln K_{nm}$, was calculated as a difference in the logarithms of the reduced partition function ratio, β, of U^{IV}, U^{V} and U^{VI}, e.g.:

$$\ln K_{\mathrm{nm}} = \ln\beta\left(\mathrm{U^V}\right) - \ln\beta\left(\mathrm{U^{VI}}\right) \qquad \text{(Eq. S-2)}$$

U M_4-edge HR-XANES spectroscopy

U M_4-edge HR-XANES spectra were recorded at the station for actinide science (ACT) at the CAT-ACT beamline at the Karlsruhe Research Accelerator (KARA), Karlsruhe, Germany, which is equipped with a Johann type X-ray emission spectrometer (Zimina *et al.*, 2017). Spectra were collected as described previously (Molinas *et al.*, 2021), and data processing and normalisation was performed using the ATHENA software (Ravel and Newville, 2005).

Equilibrium isotope exchange between U^V-dpaea and the U^{IV} product

Abiotic equilibrium isotope exchange between U^V and U^{IV} was determined during the reaction between ~110 µM U^V-dpaea with an initial isotopic composition of ~5‰, and ~57 µM U^{IV} present as the product of the bioreduction experiments of natural U, with an initial isotopic composition of 0‰. The U speciation was maintained using the same medium composition as for bioreduction experiments. Bacterial cells were inactivated via sonication to ensure no further biologically-mediated redox change. Samples were filtered through 0.22 µm filters and U concentrations and isotope signatures were determined by ICP-MS and MC-ICP-MS, respectively.

Supplementary Figures

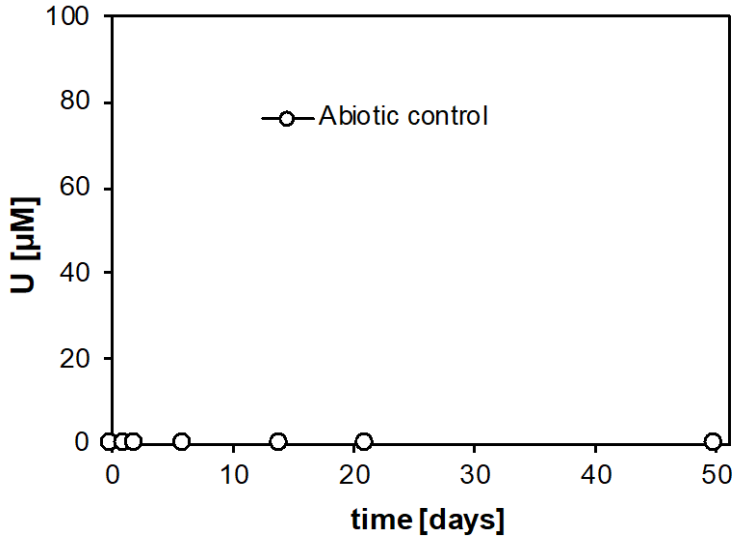

Figure S-1 Aqueous uranium concentrations in abiotic control experiments. Samples were filtered through 0.22 µm filters. Symbols depict the mean of duplicate reactors and error bars show 1 standard deviation of the mean. Where not visible, the error is smaller than the symbol size.

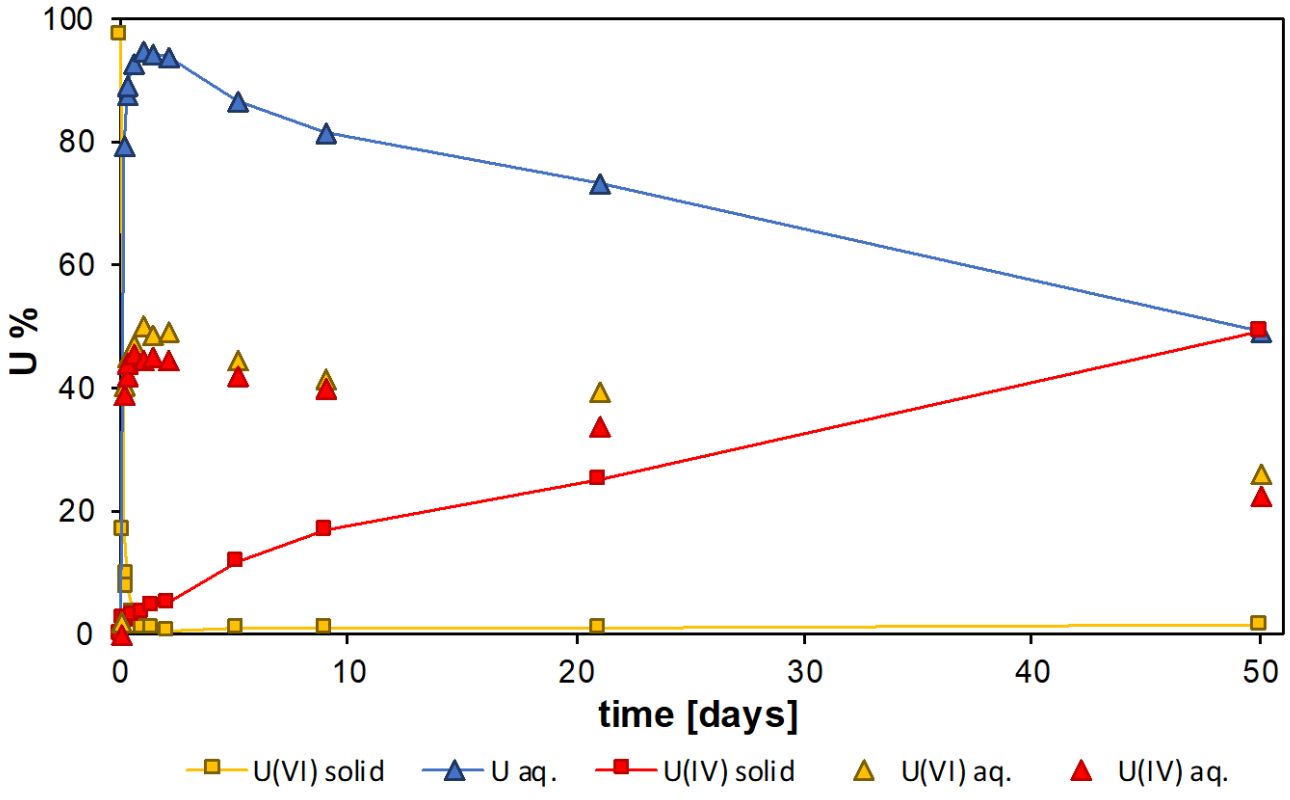

Figure S-2 Uranium mass distribution in a series of sacrificial reactors. The aqueous uranium (blue triangles) was acidified with 4.5 N HCl and immediately underwent anion exchange chromatography to quantitatively separate U^{IV} (red triangles) and U^{VI} (yellow triangles). The $\delta^{238}U$ values of each valence state of the 48-h sample were −0.04 ± 0.04 ‰ and 0.03 ± 0.02 ‰, respectively.

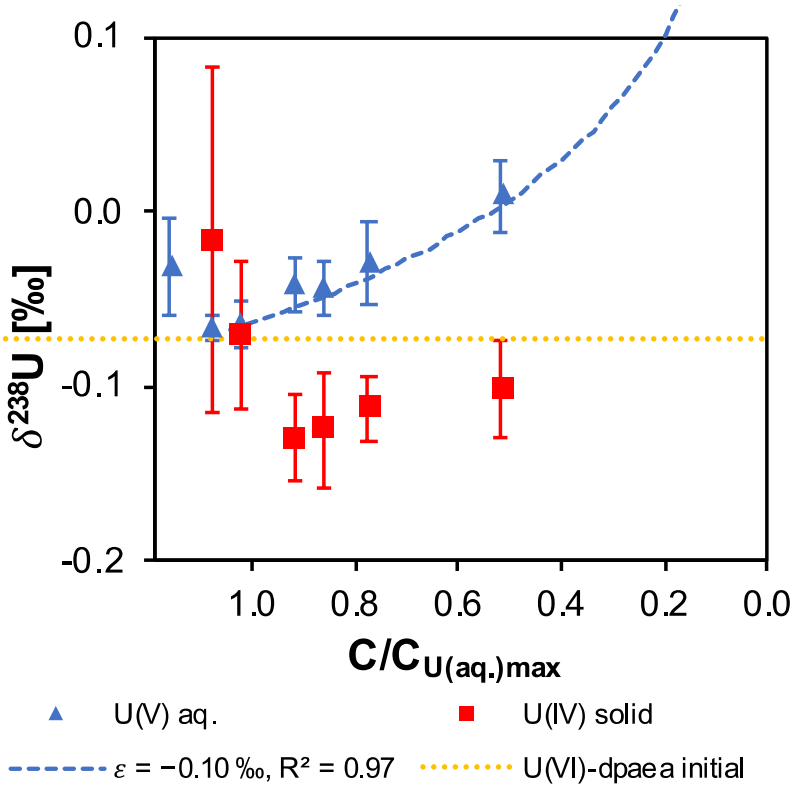

Figure S-3 δ^{238}U values for each of the U components as a function of the aqueous U^{V} concentration, reported as a fraction of the maximum U^{V} concentration. These data correspond to the concentration data reported in Figure 1a. Symbols and error bars depict two standard deviations of the mean of triplicate measurements. The Rayleigh model (blue dashed line) of the δ^{238}U values of U^{V} correspond to the linear best fit of the logarithmic data, R^2 = 0.97, from which the isotope enrichment factor, ε, is derived. The δ^{238}U value of the initial U^{VI}-dpaea is plotted as a yellow dotted line.

Supplementary Table

Table S-1 $\ln K_{fs}$ (nuclear field shift effect term), $\ln K_{nm}$ (nuclear mass term) and ε^{eq} (total fractionation factor) for the reduction of U^{VI} to U^{V} and that of U^{V} to U^{IV}. $\ln K_{fs}$ was calculated by either X2C-Hartree-Fock (X2C-HF) or X2C-B3LYP, and the values are shown in the columns of "HF" and "B3LYP", respectively. Likewise, the total fractionation factor is shown for both calculation methods of $\ln K_{fs}$. All values are shown in units of ‰ (permil). The computational methods are described above.

Reaction	$\ln K_{fs}$		$\ln K_{nm}$	ε^{eq}	
	HF	B3LYP		HF	B3LYP
$U^{VI}O_2$-dpaea ⟶ $U^{V}O_2$-dpaea$^-$	1.98	1.21	−0.39	1.60	0.82
$U^{V}O_2$-dpaea$^-$ ⟶ U^{IV}-(dpaea)$_2$	0.96	1.01	−0.68	0.27	0.33
$U^{V}O_2$-dpaea$^-$ ⟶ $CaU^{IV}(PO_4)_2$	1.04	0.71	−0.58	0.46	0.13

Supplementary Information References

Alessi, D.S., Lezama-Pacheco, J.S., Stubbs, J.E., Janousch, M., Bargar, J.R., Persson, P., Bernier-Latmani, R. (2014) The product of microbial uranium reduction includes multiple species with U(IV)-phosphate coordination. *Geochimica et Cosmochimica Acta* 131, 115–127. https://doi.org/10.1016/j.gca.2014.01.005

Bernier-Latmani, R., Veeramani, H., Vecchia, E.D., Junier, P., Lezama-Pacheco, J.S., Suvorova, E.I., Sharp, J.O., Wigginton, N.S., Bargar, J.R. (2010) Non-uraninite products of microbial U (VI) reduction. *Environmental Science and Technology* 44, 9456–9462. https://doi.org/10.1021/es101675a

Brown, A.R., Roebbert, Y., Sato, A., Hada, M., Abe, M., Weyer, S., Bernier-Latmani, R. (2023) Contribution of the nuclear field shift to kinetic uranium isotope fractionation. *Geochemical Perspectives Letters* 27, 43–47. https://doi.org/10.7185/geochemlet.2333

Faizova, R., Scopelliti, R., Chauvin, A.-S., Mazzanti, M. (2018) Synthesis and characterization of a water stable uranyl(V) complex. *Journal of the American Chemical Society* 140, 13554–13557. https://doi.org/10.1021/jacs.8b07885

Molinas, M. Faizova, R., Brown, A., Galanzew, J., Schacherl, B., Bartova, B., Meibom, K.L., Vitova, T., Mazzanti, M. and Bernier-Latmani, R. (2021) Biological reduction of a U(V)-organic ligand complex. *Environmental Science and Technology* 55, 4753–4761. https://doi.org/10.1021/acs.est.0c06633

Molinas, M., Meibom, K.L., Faizova, R., Mazzanti, M., Bernier-Latmani, R. (2023) Mechanism of reduction of aqueous U(V)-dpaea and solid-phase U(VI)-dpaea complexes: The role of multiheme *c*-type cytochromes. *Environmental Science and Technology* 57, 7537–7546. https://doi.org/10.1021/acs.est.3c00666

Ravel, B., Newville, M. (2005) ATHENA, ARTEMIS, HEPHAESTUS: Data analysis for X-ray absorption spectroscopy using IFEFFIT. *Journal of Synchrotron Radiation* 12, 537–541. https://doi.org/10.1107/S0909049505012719

Richter, S., Alonso-Munoz, A., Eykens, R., Jacobsson, U., Kuehn, H., Verbruggen, A., Aregbe, Y., Wellum, R., Keegan, E. (2008) The isotopic composition of natural uranium samples—Measurements using the new n(^{233}U)/n(^{236}U) double spike IRMM-3636. *International Journal of Mass Spectrometry* 269, 145–148. https://doi.org/10.1016/j.ijms.2007.09.012

Russell, W.A., Papanastassiou, D.A., Tombrello, T.A. (1978) Ca isotope fractionation on the Earth and other solar system materials. *Geochimica et Cosmochimica Acta* 42, 1075–1090. https://doi.org/10.1016/0016-7037(78)90105-9

Sato, A., Bernier-Latmani, R., Hada, M., Abe, M. (2021) *Ab initio* and steady-state models for uranium isotope fractionation in multi-step biotic and abiotic reduction. *Geochimica et Cosmochimica Acta* 307, 212–227. https://doi.org/10.1016/j.gca.2021.05.044

Scott, K.M., Lu, X., Cavanaugh, C.M., Liu, J.S. (2004) Optimal methods for estimating kinetic isotope effects from different forms of the Rayleigh distillation equation. *Geochimica et Cosmochimica Acta* 68, 433–442. https://doi.org/10.1016/S0016-7037(03)00459-9

Stoliker, D.L., Campbell, K.M., Fox, P.M., Singer, D.M., Kaviani, N., Carey, M., Peck, N.E., Bargar, J.R., Kent, D.B., Davis, J.A. (2013a) Evaluating chemical extraction techniques for the determination of uranium oxidation state in reduced aquifer sediments. *Environmental Science and Technology* 47, 9225–9232. https://doi.org/10.1021/es401450v

Stoliker, D.L., Kaviani, N., Kent, D.B., Davis, J.A. (2013b) Evaluating ion exchange resin efficiency and oxidative capacity for the separation of uranium(IV) and uranium(VI). *Geochemical Transactions* 14, 1. https://doi.org/10.1186/1467-4866-14-1

Wang, X., Johnson, T.M., Lundstrom, C.C. (2015a) Low temperature equilibrium isotope fractionation and isotope exchange kinetics between U(IV) and U(VI). *Geochimica et Cosmochimica Acta* 158, 262–275. https://doi.org/10.1016/j.gca.2015.03.006

Wang, X., Johnson, T.M., Lundstrom, C.C. (2015b) Isotope fractionation during oxidation of tetravalent uranium by dissolved oxygen. *Geochimica et Cosmochimica Acta* 150, 160–170. https://doi.org/10.1016/j.gca.2014.12.007

Weyer, S., Anbar, A.D., Gerdes, A., Gordon, G.W., Algeo, T.J., Boyle, E.A. (2008) Natural fractionation of ^{238}U/^{235}U. *Geochimica et Cosmochimica Acta* 72, 345–359. https://doi.org/10.1016/j.gca.2007.11.012

Zimina, A., Dardenne, K., Denecke, M.A., Doronkin, D.E., Huttel, E., Lichtenberg, H., Mangold, S., Pruessmann, T., Rothe, J., Spangenberg, T., Steininger, R., Vitova, T., Geckeis, H., Grunwaldt, J.D. (2017) CAT-ACT - A New Highly Versatile x-Ray Spectroscopy Beamline for Catalysis and Radionuclide Science at the KIT Synchrotron Light Facility ANKA. *Review of Scientific Instruments* 88, 113. https://doi.org/10.1063/1.4999928